Two-photon bistable switching of an optically pumped atomic neon Raman laser

X.-W. Xia,* W. J. Sandle, R. J. Ballagh,† and D. M. Warrington
Physics Department, University of Otago, Dunedin, New Zealand
(Received 1 August 1995)

Two cw Raman lines at 603.0 nm ($2p_2 \rightarrow 1s_4$) and 659.9 nm ($2p_2 \rightarrow 1s_2$), generated when cw dye-laser radiation is mode matched to the 588.2-nm ($1s_5 \rightarrow 2p_2$) transition of Ne I in a commercial He-Ne laser cavity, can both show optically bistable switching simultaneously with the pump beam. A theoretical treatment based on a semiclassical three-state Raman laser model is used to qualitatively reproduce the experimental observations and to identify the mechanisms that produce the experimental signature. Important features of the Raman gain are characterized. These, in combination with the phase-shift properties of the pump and Raman fields, are used to explain the switching behavior.

PACS number(s): 42.50.−p, 42.60.−v, 42.65.−k

I. INTRODUCTION

Two-photon processes possess an intrinsic nonlinear character that can be exploited in many quantum and nonlinear optical phenomena. Arecchi and Politi [1] first suggested that optical switching processes could be based on two-photon absorption and subsequently the theory has attracted considerable attention (e.g., [2–8]), although experiments have been rather fewer [9–13]. Polarization switching [14–16] also involves two distinct photons, but in common with two-photon absorption, it is a passive process in which the frequencies of the photons are predetermined and fixed by the input field. The Raman laser, on the other hand, is a distinctively different two-photon process in that the second (i.e., Raman) photon establishes its own frequency by interaction of the two-photon nonlinear response (both the gain and the dispersion) and the cavity resonance condition. In a series of papers, Harrison and co-workers [17–20] have studied both experimental and theoretical aspects of the dynamics, bistability, and switching of Raman lasers and an experiment has also been reported by Zheng and Cao [21]. Both experiments operated in a regime where the pump behavior could be ignored and the theories used assumed negligible pump depletion (e.g., [18–20]).

In the present paper we report (in Sec. II) the observation of two-photon optical switching by a neon Raman laser, optically pumped close to atomic resonance by a dye laser, mode matched to the Raman laser cavity. We have utilized Raman gain found previously in neon between the 1*s* and 2*p* manifolds (Paschen notation) in a standard, commercial, operating He-Ne laser [22]. In contrast to the previous Raman switching observations [17,21], our experiment involves the pump in an essential way, and variations of the pump intensity (which occur mainly due to cavity resonance effects) have a major effect on the output Raman behavior. By analyzing (Sec. III) a theoretical model that incorporates both pump depletion by the two-photon interaction and cavity resonance effects, we are able (in Sec. IV) to identify the key physical mechanisms and to explain their interactions that lead to the observed switching.

II. EXPERIMENT AND RESULTS

The experimental arrangement is essentially identical to that described in our previous work (see Fig. 2 of Ref. [22]), where gain on a number of Raman lines between neon 1*s* and 2*p* manifolds was reported. A linearly polarized pump beam from a CR-699-21 dye laser is mode matched to the He-Ne ''cell cavity'' (NEC GLT-172, of free spectral range 667 MHz) through its higher (0.8%) transmittance mirror $M1$. In the present work the He-Ne laser cavity serves three separate functions: supporting the standard 633-nm emission (which does not have a scientific role in this work, although we do use the 633-nm output to stabilize the cavity length); providing feedback to enable lasing at either or both Raman wavelengths of 603.0 nm ($2p_2 \rightarrow 1s_4$) and 659.9 nm ($2p_2 \rightarrow 1s_2$); and acting as a ''buildup cavity'' in which the optical pump nonlinearly, and near-resonantly, drives the single-photon 588.2-nm ($1s_5 \rightarrow 2p_2$) transition and provides gain for the Raman lines. Under conditions of no discharge, the cavity finesse at 588.2 nm is approximately 220. A blazed grating ($G1$) just before mirror $M1$ allows spatial separation of the retroreflected dye-laser beam and the coherent emissions from the cavity: the 633-nm cell-laser beam and the Raman lasing lines. A further grating ($G2$) permits spatial separation of the beams emerging from the lower transmittance (0.01%) mirror $M2$. Using the 633-nm cell-laser beam diffracted by grating $G1$ and standard locking techniques, the cell cavity is frequency stabilized to an enclosed reference cavity, which is itself locked to a frequency-stabilized He-Ne reference laser. A Brewster plate mounted in the reference cavity on a scanning galvanometer passes only the cell-laser beam, so the cell-cavity resonance frequency can be scanned under its gain profile—using a heating wire for thermal expansion control—by having it track the reference cavity. The time constant of the locking loop is several seconds. A photovoltaic-mediated interaction with the 633-nm line

*Present address: Photodynamic Research Center, The Institute of Physical and Chemical Research, 19-1399 Koeji, Nagamachi, Aoba-ku, Sendai, Miyagi 980, Japan.
†On leave at Physics Department, Faculties, Australian National University, Canberra, Australia.

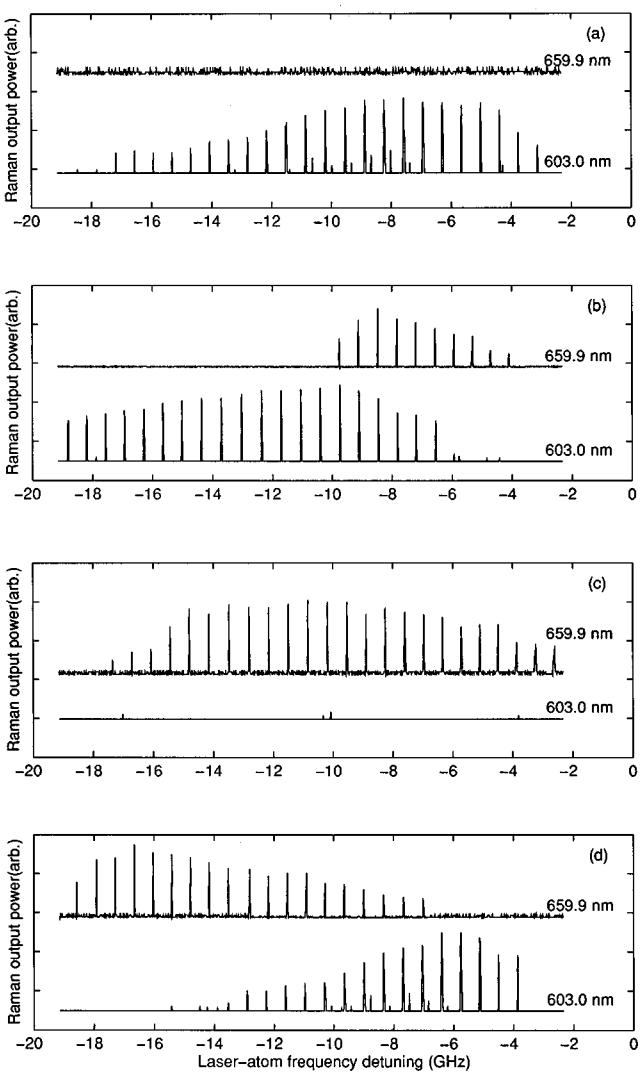

FIG. 1. Simultaneous measurements of output powers for the two observed Raman lines at 603.0 and 659.9 nm when the pump frequency is swept across a number of cavity resonances immediately below the 588.2-nm atomic-line center. The cavity length increases successively by a few wavelengths for each step in the progression from (a) to (d); all other conditions remain the same. Input power, 100 mW; neon discharge current, 4.8 mA.

meant that locking was upset when the dye laser was tuned for more than a few seconds to a cavity resonance near the $1s_5 \rightarrow 2p_2$ line. However, this did not prevent locking during frequency scans of the dye laser across a number of cavity profiles, which are the experimental results of main interest. Presumably, the reduction in the time for which the circulating pump intensity was large and the relatively rapid passage through cavity resonances meant that the locking assumed an average, stable, configuration.

An associated problem that arose was the difficulty of establishing precise, absolute values of the cavity optical length. As we shall see below, measuring laser detuning from the nearest cavity resonance, which is the usual cavity length requirement for determining switching behavior, provides insufficient information to predict behavior in this present experiment.

In Fig. 1 we present a typical set of Raman outputs at 603.0 and 659.9 nm occurring as the dye laser is frequency scanned by about 20 GHz immediately below the 588.2-nm line center. The only change between the four separate sets of data is that the cavity length is adjusted by a total of less than ten wavelengths of the 588.2-nm line. It can be seen that the change of cavity length has a dramatic effect on the Raman outputs and is one of the main features of our experimental results. Initially [see Fig. 1(a)] the 659.9-nm output is suppressed and the 603.3 nm appears almost every time the pump field builds at a cavity resonance. (The secondary small peaks in the center region of the plot are from off-axis modes that have not been completely suppressed in the mode-matching process.) Then, for a cavity length increased by approximately three (588.2 nm) wavelengths [Fig. 1(b)], the 659.9-nm line begins to appear, while the envelope at 603.0 nm is moved down in frequency. The next length increase [Fig. 1(c)] leads to the 603.0-nm emission being suppressed and the 659.9-nm lasing at almost every cavity resonance; finally [Fig. 1(d)], the 603.0 nm reappears and the 659.9 nm shifts down in frequency. Further cavity length increases lead to an approximate repetition of the pattern (but with different periods for appearance of the two Raman wavelengths).

At the simplest level, the appearance and disappearance of the Raman ''combs'' as cavity length is changed can be easily understood. For stimulated Raman emission to occur, the pump laser must be tuned to one of the longitudinal modes of the cavity and the Raman must be near resonant to another. As a first approximation, the Raman frequency is determined by the two-photon resonance condition [see Eq. (19)], thus requiring that the initial-to-final-state (''two-photon'') frequency separation ω_{21} [see Fig. 5(a)] be an integral number of free spectral ranges of the cavity. For both Raman lines to simultaneously lase, both of the corresponding two-photon frequency splittings should simultaneously ''resonate'' with the cavity. In theory, this cannot occur exactly, because the two frequency splittings are incommensurate. However, frequency pulling effects associated with the nonlinear interactions provide a measure of flexibility and in fact play a major role in determining the Raman behavior, as we discuss in Sec. IV.

We now turn to a brief survey of the types of switching that can occur. First, if cavity length and laser-atom detuning are chosen to avoid Raman lasing altogether, then for sufficient dye laser power, normal optical bistability, very similar to that obtained in Ref. [23], results. The next most simple switching involves a single Raman lasing line. Figure 2(a) illustrates a case where only the 603.0-nm line is lasing and Fig. 2(b) where the only line lasing is 659.9 nm. These correspond to nearly exact two-photon resonance in each individual case: the Raman line ''turns on'' when the pump builds up to a critical threshold and ''turns off'' abruptly as the pump switches to the lower branch. There is some, but not pronounced, evidence of the intracavity pump power being modified as the Raman field switches on.

Modification to the pump *is* pronounced in the case shown in Fig. 3. Here the Raman line is not initially resonant with the cavity, but is pulled into resonance by the two-photon interaction. Further discussion is given in Sec. IV, where the mechanisms involved are outlined in some detail. Finally, in Fig. 4 we show a case where the Raman lines may

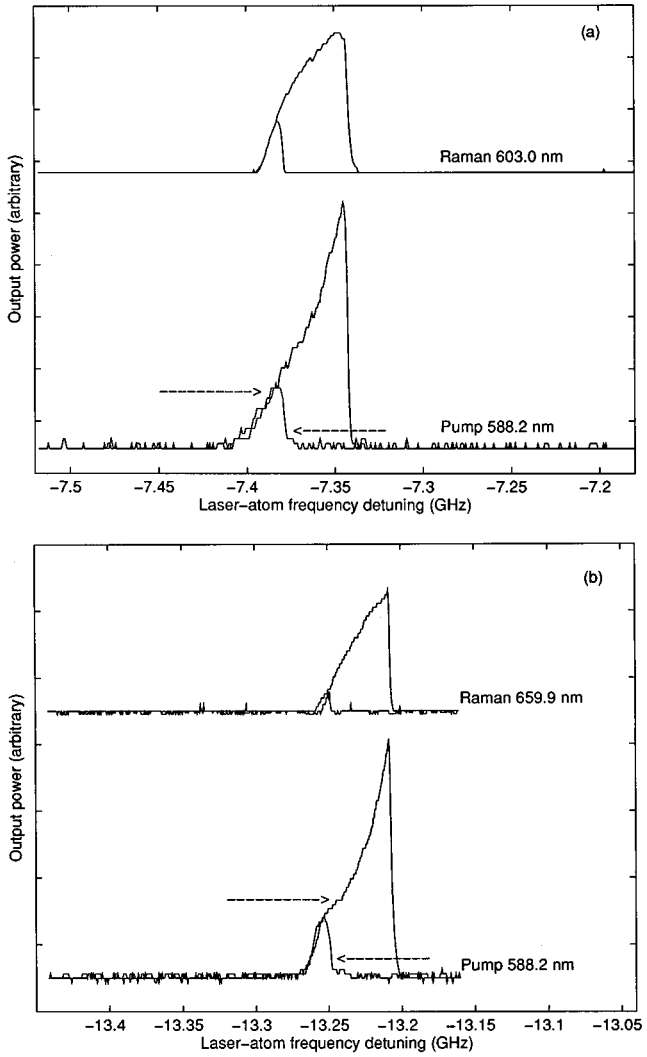

FIG. 2. Forward and backward frequency scanning showing simultaneous optical bistable switching for (a) both the pump and Raman 603.0-nm emission with pump input power 106 mW and (b) both the pump and Raman 659.9-nm emission with pump input power 131 mW. Both the cavity length and laser-atom detuning differ between (a) and (b).

simultaneously coexist. The cavity length is such as to somewhat favor the generation of the 603.0-nm line, but as the pump frequency is further tuned, the 659.9-nm line can also become near resonant with its corresponding cavity resonance and shows behavior similar to Fig. 2. Figure 4 shows clearly how the intracavity pump power can be modified, with the pump profile showing a deep valley after the 603.3-nm Raman emission turns on. On the other hand, direct competition between the two Raman lines, other than mediated via pump depletion, does not appear to be particularly significant.

III. THEORY

In order to understand the above results, we consider a semiclassical three-state Λ model [Fig. 5(a)] for the coupled Raman-pump system in which, like Uppal, Harrison, and Lu [24] for the on-resonant case, pump depletion is included. Our treatment, however, is not confined to a resonant situation. A single Raman line only is modeled; we expect coupling between different Raman outputs to be relatively unimportant, so that the two-Raman case could be considered as two independent Raman processes. A gas of homogeneously broadened three-state atoms [Fig. 5(a)] is confined between $z=0$ and L inside a ring cavity of length L [Fig. 5(b)] with input and output mirrors each of reflectance R and transmittance $(1-R)$. The electric field inside the cavity is the sum of pump $\mathscr{E}_p(\mathbf{r},t)$ and Raman $\mathscr{E}_r(\mathbf{r},t)$ fields

$$\begin{aligned}\mathscr{E}(\mathbf{r},t)&=\mathscr{E}_p(\mathbf{r},t)+\mathscr{E}_r(\mathbf{r},t)\\&=\{\hat{\boldsymbol{\varepsilon}}_p E_p(\mathbf{r},t)\exp[-i(\omega_p t-k_p z)]\\&\quad+\hat{\boldsymbol{\varepsilon}}_r E_r(\mathbf{r},t)\exp[-i(\omega_r t-k_r z)]\}+\text{c.c.},\end{aligned}\tag{1}$$

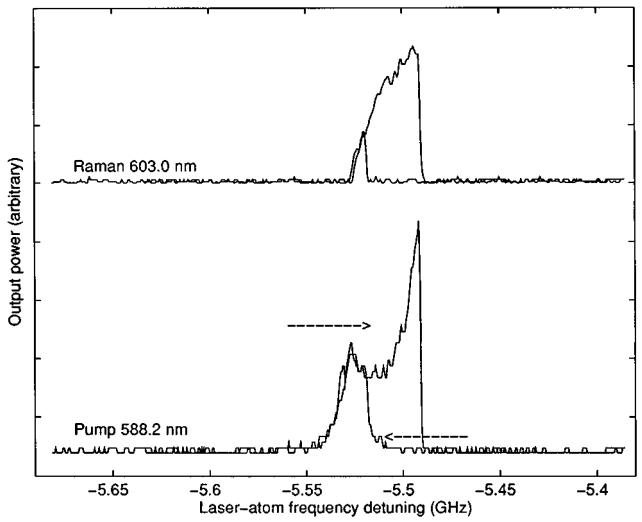

FIG. 3. Forward and backward frequency scanning showing simultaneous optical bistable switching and hysteresis for both the pump transmission and the Raman 603.0-nm emission under conditions of significant pump depletion. Pump input power, 164 mW; neon discharge current, 4.8 mA.

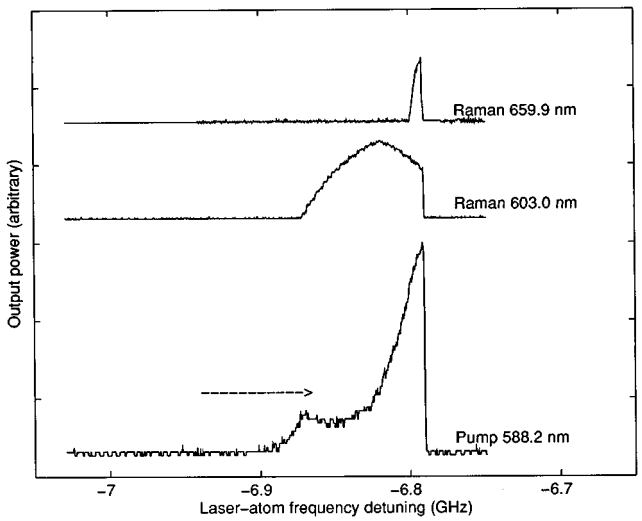

FIG. 4. Forward frequency scan showing switching for both Raman 603.0- and 659.9-nm lines simultaneously with the pump 588.2-nm transmission. The 603.0-nm Raman radiation has a wider profile and turns on at a lower frequency than the 659.9-nm line. Pump input power, 121 mW; neon discharge current, 4.5 mA.

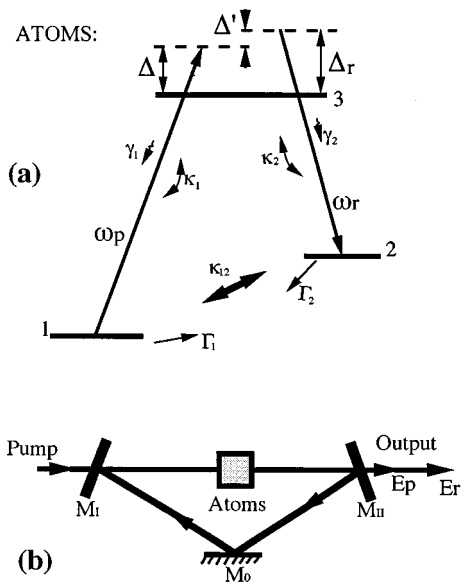

FIG. 5. Three-state Raman laser model. (a) Three-state Λ structure atoms with decay rates and detunings. The frequency separations between levels 2 and 1, 3 and 1, and 3 and 2 are, respectively, ω_{21}, ω_{31}, and ω_{32}. (b) Unidirectional ring-cavity model.

where $\hat{\boldsymbol{\varepsilon}}_p$ and $\hat{\boldsymbol{\varepsilon}}_r$ are unit vectors indicating polarization directions and k_p and k_r are the vacuum wave vectors associated with the pump and Raman frequencies $k_p=\omega_p/c$ and $k_r=\omega_r/c$. The positive-frequency complex amplitudes $E_p(\mathbf{r},t)$ and $E_r(\mathbf{r},t)$ are slowly varying field envelopes.

The pump and Raman frequency detunings from their respective atomic transitions $\Delta=\omega_p-\omega_{31}$ and $\Delta_r=\omega_r-\omega_{32}$ are shown in Fig. 5(a) together with the nominal two-photon detuning from exact two-photon resonance $\Delta'=\Delta_r-\Delta=\omega_{21}-(\omega_p-\omega_r)$. It is assumed that each field mode interacts with a single optical transition, so that the couplings of the fields with the atomic dipoles $\boldsymbol{\mu}_{13}$ $(=\langle 1|\boldsymbol{\mu}|3\rangle)$ and $\boldsymbol{\mu}_{23}$ $(=\langle 2|\boldsymbol{\mu}|3\rangle)$ are characterized simply by (the two complex half-Rabi frequencies)

$$\alpha=\boldsymbol{\mu}_{31}\cdot\hat{\boldsymbol{\varepsilon}}_p E_p/\hbar, \quad \beta=\boldsymbol{\mu}_{32}\cdot\hat{\boldsymbol{\varepsilon}}_r E_r/\hbar. \tag{2}$$

The density-matrix equations can be written in terms of slowly varying, off-diagonal elements $\tilde{\rho}_{31}=\exp[i(\omega_p t-k_p z)]\rho_{31}$, $\tilde{\rho}_{32}=\exp[i(\omega_r t-k_r z)]\rho_{32}$, and $\tilde{\rho}_{21}=\exp\{i[(\omega_p-\omega_r)t-(k_p-k_r)z]\}\rho_{21}$ and population differences $D_{ij}=\rho_{ii}-\rho_{jj}$ as

$$\dot{\tilde{\rho}}_{31}=-(\kappa_1-i\Delta)\tilde{\rho}_{31}-i\alpha D_{31}+i\beta\tilde{\rho}_{21}, \tag{3a}$$

$$\dot{\tilde{\rho}}_{32}=-(\kappa_2-i\Delta_r)\tilde{\rho}_{32}-i\beta D_{32}+i\alpha\tilde{\rho}_{21}^*, \tag{3b}$$

$$\dot{\tilde{\rho}}_{21}=-[1-i(\Delta-\Delta_r)]\tilde{\rho}_{21}-i\alpha\tilde{\rho}_{32}^*+i\beta^*\tilde{\rho}_{31}, \tag{3c}$$

$$\dot{D}_{31}=4\ \mathrm{Im}(\alpha^*\tilde{\rho}_{31})+2\ \mathrm{Im}(\beta^*\tilde{\rho}_{32})+r_0+r_1D_{31}+r_2D_{32}, \tag{3d}$$

$$\dot{D}_{32}=2\ \mathrm{Im}(\alpha^*\tilde{\rho}_{31})+4\ \mathrm{Im}(\beta^*\tilde{\rho}_{32})+s_0+s_1D_{31}+s_2D_{32}, \tag{3e}$$

where we have set

$$r_0=\frac{\Gamma_1-\Gamma_2-2\gamma_1-\gamma_2}{3}, \quad r_1=-\frac{2\Gamma_1+\Gamma_2+2\gamma_1+\gamma_2}{3},$$

$$r_2=\frac{\Gamma_1+2\Gamma_2-2\gamma_1-\gamma_2}{3}$$

and

$$s_0=-\frac{\Gamma_1-\Gamma_2+\gamma_1+2\gamma_2}{3}, \quad s_1=\frac{2\Gamma_1+\Gamma_2-\gamma_1-2\gamma_2}{3},$$

$$s_2=-\frac{\Gamma_1+2\Gamma_2+\gamma_1+2\gamma_2}{3}. \tag{4}$$

κ_1 and κ_2 are the optical-dipole dephasing rates for the pump and Raman transitions respectively; γ_1 and γ_2 are the population decay rates from the upper level 3 to the lower levels 1 and 2; Γ_1 and Γ_2 are the population transfer rates from level 1 to 2 and from 2 to 1, respectively. All rates and frequencies are scaled with respect to the Raman coherence decay rate κ_{12} and time is in units of κ_{12}^{-1}.

We note that the full density-matrix equations and the analytical solutions for a closed three-level system have been given by Ryan and Lawandy [25]. The total macroscopic polarization is

$$\begin{aligned}\mathscr{P}(z,t)&=N\ \mathrm{Tr}(\boldsymbol{\mu}\rho)\\&=N\{\boldsymbol{\mu}_{13}\tilde{\rho}_{31}\exp[-i(\omega_p t-k_p z)]\\&\quad+\boldsymbol{\mu}_{23}\tilde{\rho}_{32}\exp[-i(\omega_r t-k_r z)]\}+\mathrm{c.c.},\end{aligned} \tag{5}$$

where N is the atomic density.

Using the slowly varying envelope approximation and the cavity *mean-field* assumption (e.g., Refs. [26,27]) the Maxwell-Bloch equations for the pump and Raman cavity fields become

$$\frac{d\alpha}{dt}=-\kappa\alpha+ig_1\tilde{\rho}_{31}+i\Phi_1\alpha+\kappa\alpha_s \tag{6}$$

and

$$\frac{d\beta}{dt}=-\kappa\beta+ig_2\tilde{\rho}_{32}+i(\Phi_2+\Delta')\beta. \tag{7}$$

Here κ is the cavity decay rate (in units of κ_{12}) and the gain parameters g_1 (for pump) and g_2 (for Raman) are defined by

$$g_i=2\kappa\kappa_i C_i, \tag{8}$$

where the cooperativities are

$$C_i=\frac{\alpha_{0i}L}{4(1-R)} \quad (i=1,2), \tag{9}$$

with α_{0i} the weak-field, resonant absorption coefficients for (homogeneously broadened) pump and Raman transitions

$$\alpha_{01}=\frac{N|\boldsymbol{\mu}_{13}|^2\omega_p}{\varepsilon_0 c\hbar\kappa_1}, \quad \alpha_{02}=\frac{N|\boldsymbol{\mu}_{23}|^2\omega_r}{\varepsilon_0 c\hbar\kappa_2}. \tag{10}$$

Φ_1 is the laser-cavity detuning (in units of κ_{12}) defined by

$$\Phi_1=\omega_p-\omega_{cp}, \tag{11}$$

where ω_{cp} is the empty-cavity resonance frequency nearest to ω_p.

The detuning of the Raman frequency from its nearest cavity frequency ω_{cr} is $(\omega_r-\omega_{cr})$, but since ω_r is free to vary, we define Φ_2 as

$$\Phi_2=(\omega_p-\omega_{21})-\omega_{cr}, \tag{12}$$

which represents the cavity detuning of the nominal Raman frequency $\omega_p-\omega_{21}$ in units of κ_{12}. We remark that the validity of Eqs. (6) and (7) requires that Φ_1 and $\Phi_2+\Delta'$ are both small compared to a free spectral range. Finally, from the input pump half-Rabi frequency α_{input} (outside the cavity) we obtain the scaled input field

$$\alpha_s=\alpha_{\text{input}}/\sqrt{1-R}. \tag{13}$$

For reference, we note that the output fields are obtained from the cavity fields via $\alpha_{\text{output}}=\alpha\sqrt{1-R}$ and $\beta_{\text{output}}=\beta\sqrt{1-R}$.

IV. NUMERICAL RESULTS AND DISCUSSION

Equations (3), (6), and (7) are the basic equations of our model and we have solved these to obtain steady-state system behavior using the AUTO bifurcation-analysis software package [28]. We shall see that the simulation reproduces the Raman-comb behavior of Fig. 1 (which is the main signature of the experiment) and enables us to understand the mechanisms responsible for the behavior seen in Figs. 1–3. We begin, in Fig. 6, by presenting the results of simulations in which a pump field of constant input intensity is frequency scanned through a number of cavity resonances from well below to just above pump-atom resonance. Parameters have been chosen to relate the model closely to the experiment for 603-nm Raman emission, as discussed in the Appendix. Three separate scan simulations were performed, corresponding to successively increasing the cavity round-trip length L by two pump wavelengths each time. Note that the value of Φ_1 for a given Δ is unchanged and also that, for a given cavity length, $\Phi_1-\Phi_2$ is constant across all peaks of an entire frequency scan. Thus we can represent the effect of the cavity length change by setting the cavity detunings (at $\Delta=-400$) to $\Phi_1=-2.0$ and $\Phi_2=3.3$ in the first scan, $\Phi_1=-2.0$ and $\Phi_2=2.5$ in the second scan, and $\Phi_1=-2.0$ and $\Phi_2=1.7$ in the third. [The change in Φ_2 per pump-wavelength increase in L is the free spectral range (in units of κ_{12}) times the factor $(1-\lambda_{\text{pump}}/\lambda_{\text{Raman}})$.] The output pump amplitude for the first scan is shown in Fig. 6(a) and the broad feature of the power broadened atomic response is seen in the decreasing peak transmission as the pump scans towards resonance. At the level of detail shown in the figure, the *pump* output-frequency combs for the second and third scans do not differ appreciably from the first and hence are not repeated. The *Raman* amplitudes, however, change dramatically from the first scan [Fig. 6(b)] to the third [Fig. 6(d)], showing the considerable sensitivity of Raman lasing range to cavity length, thus confirming that the theory reproduces the main features of the experiment.

In order to understand the main physical mechanisms at play, it is convenient to define a coupling coefficient for the pump field as

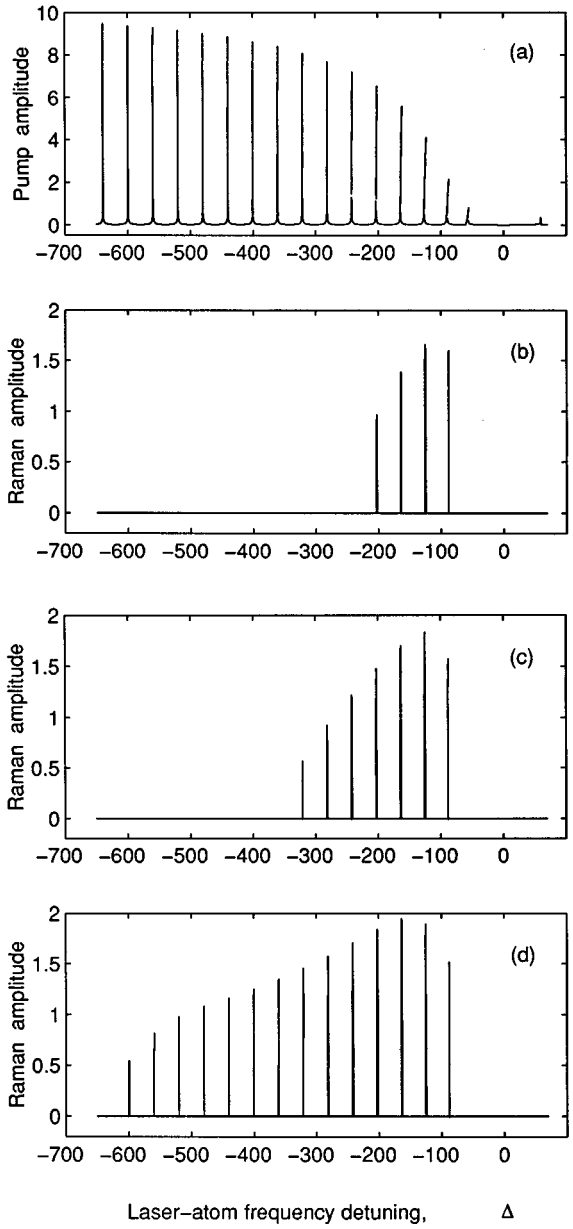

FIG. 6. Theoretical simulations of pump frequency scans corresponding to three different cavity lengths: (a) the intracavity pump amplitude $|\alpha|$ (essentially unchanged for each scan), (b) the intracavity Raman amplitude $|\beta|$ for the case $\Phi_1=-2.0$ and $\Phi_2=3.3$, (c) the Raman amplitude for the case $\Phi_1=-2.0$ and $\Phi_2=2.5$, and (d) the Raman amplitude for the case $\Phi_1=-2.0$ and $\Phi_2=1.7$. The Φ values are each referenced to $\Delta=-400$ and in every case $\alpha_s=10.3$, $\kappa_1=1.1$, $\kappa_2=0.9$, $\gamma_1=0.04$, $\gamma_2=0.02$, $\Gamma_1=8.9\times10^{-5}$, $\Gamma_2=1.07\times10^{-3}$, $\kappa=0.03$, $g_1=1200$, and $g_2=1500$.

$$\eta=-ig_1\tilde{\rho}_{31}/\alpha. \tag{14}$$

In terms of η, the steady-state equation for the intracavity pump field is given by the implicit equation

$$|\alpha|^2=\frac{\kappa^2}{[\kappa+\text{Re}(\eta)]^2+[\Phi_1-\text{Im}(\eta)]^2}|\alpha_s|^2, \tag{15}$$

so that it is evident that $\mathrm{Re}(\eta)$ is the loss coefficient and $\mathrm{Im}(\eta)$ the dispersive phase shift (or frequency pulling) for the pump field. We may similarly define a coupling coefficient for the Raman field as

$$\eta_r = -ig_2\tilde{\rho}_{32}/\beta, \tag{16}$$

in terms of which the Raman gain coefficient for the medium is given by $-\mathrm{Re}(\eta_r)$ and the Raman phase shift (or frequency pulling) is given by $\mathrm{Im}(\eta_r)$.

In the absence of the Raman field $\beta=0$ (which applies, for example, in the far wings of the first scan), the pump undergoes the familiar ''two-state'' optical bistability, with an expression for η in the steady state, which can be shown from Eqs. (3), (4), and (14) to have the two-state form

$$\eta = \frac{g_1(\kappa_1 + i\Delta)}{(\kappa_1^2+\Delta^2)\left(1+\dfrac{\Gamma_1}{\Gamma_2}\right) + \dfrac{2\kappa_1(\Gamma_1+2\Gamma_2+\gamma_2)}{\Gamma_2(\gamma_1+\gamma_2)}|\alpha|^2}. \tag{17}$$

The behavior of the frequency scan for the two-state case has been discussed in detail by Sandle and Gallagher [23]. However, with the three-state model, Raman lasing occurs when there is sufficient gain at a frequency ω_r, which is resonant (under the effect of the frequency pulling) with a cavity mode. Formally, this can be seen from the equation for β, Eq. (7), at steady state, which gives

$$-\mathrm{Re}(\eta_r) = \kappa \tag{18a}$$

and

$$\Delta_r - \Delta = \mathrm{Im}(\eta_r) - \Phi_2, \tag{18b}$$

where the latter is equivalent to $\omega_r = \omega_{cr} + \mathrm{Im}(\eta_r)$. To understand the implications of Eqs. (18a) and (18b), it is useful to consider the main characteristics of the Raman response function. Perhaps the single most important feature is that Raman gain will occur only when $|\Delta|$ is sufficiently large and when

$$\Delta_r \approx \frac{\Delta + \mathrm{sgn}(\Delta)\sqrt{\Delta^2 + (2|\alpha|)^2}}{2}. \tag{19}$$

The latter equation expresses the condition for (near) resonance in the two-photon pump-Raman process between the ac Stark-shifted level 1 and the bare level 2. In Fig. 7(a) the Raman gain is plotted as a function of Δ and Δ_r in the vicinity of $\Delta=-400$. We have used the same atomic-decay-rate parameters as in Fig. 6 and have chosen $\alpha=4$ and $\beta=10^{-6}$. The main feature is that the gain extends away from the line $\Delta_r=\Delta$ [i.e., Eq. (19) when $|\Delta| \gg |\alpha|$] by a width determined largely by the Raman-coherence decay rate κ_{12} (which is 1 in the present scaling). In Fig. 7(b), a contour plot traces the path in the (Δ, Δ_r) plane where gain equals cavity loss and it is at one of these lines that Raman lasing will begin. The Raman phase shift for the region corresponding to Fig. 7(a) is shown in Fig. 7(c). We note also that the pump phase shift $\mathrm{Im}(\eta)$ is slowly varying in the Δ, Δ_r region of these graphs and has a value close to -2.6.

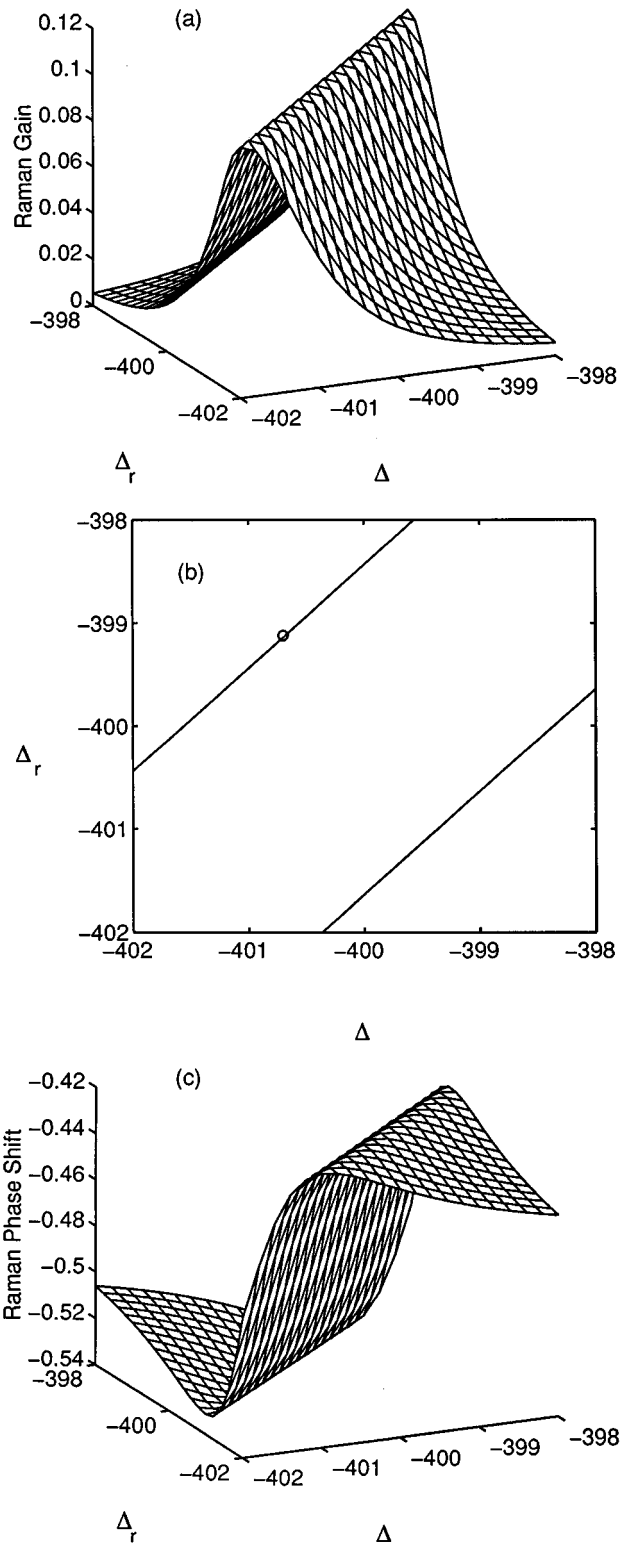

FIG. 7. Raman response as a function of pump detuning Δ and Raman detuning Δ_r with fixed pump and Raman amplitudes $\alpha=4.0$ and $\beta=10^{-6}$: (a) Raman gain, (b) paths where the Raman gain is equal to the cavity loss, and (c) Raman phase shift. The atomic and cavity decay rates are as in Fig. 6.

The detailed features of the onset of Raman lasing can be understood by referring to Fig. 8, where a theoretical scan for a single-cavity profile in the region $\Delta=-400$ is given, with system parameters the same as in Fig. 6. We have chosen

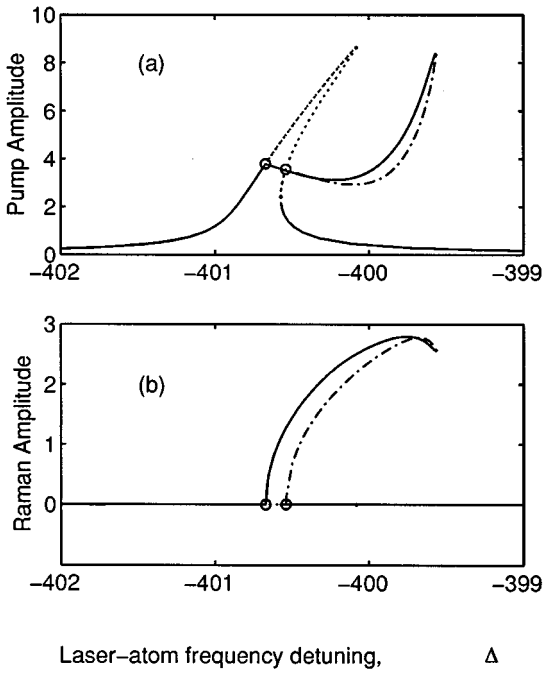

FIG. 8. Theoretical plot of (a) pump amplitude $|\alpha|$ and (b) Raman amplitude $|\beta|$ versus pump laser frequency. The solid line indicates a stable branch, the dot-dashed line an unstable branch, and the dotted lines are the solutions corresponding to zero Raman output. The threshold points for Raman lasing are indicated by circles. Parameters are as in Fig. 6, except the reference cavity detunings are $\Phi_1=-2.0$ and $\Phi_2=-1.3$ at $\Delta=-400$.

$\Phi_1=-2.0$ and $\Phi_2=-1.3$ (at $\Delta=-400$) and since the unsaturated frequency pulling for the pump is -2.8, the cavity begins to transmit the pump in the vicinity of $\Phi_1=-3.0$ (i.e., $\Delta=-401$). As the laser frequency increases and the intracavity pump intensity grows, the frequency pulling begins to bleach, so the intensity grows more slowly with frequency than it would with a linear refractive index. In the absence of Raman emission, the pump follows the dotted line. This characteristic tilted shape, familiar from two-state bistability studies [23], allows the cavity to produce different peak pump-transmission intensities depending on the direction of the frequency scan. In the present case, the dotted line represents an unstable solution; the stable solution is for Raman lasing beginning at the pump detuning of about $\Delta\approx-400.7$ and $\alpha\approx4$. At this frequency, $\Phi_1\approx-2.7$ and Raman lasing begins at the point marked by the circle in Fig. 7(b), where the corresponding Raman phase shift [see Fig. 7(c)] allows the given Raman frequency to satisfy the pulled cavity condition Eq. (18). The pump phase shift is dependent on the Raman intensity and as the Raman intensity grows, the pump phase shift suffers accelerated bleaching, with the effect that the pump is further from its dressed resonance and its transmission decreases for an interval. The Raman gain, however, decreases with increasing Raman intensity and as the Raman intensity settles to near its maximum value, the pump phase bleaching slows and the intracavity pump intensity begins to grow again. The effect of this increasing pump field is to strongly alter the Raman phase shift [to a value $\mathrm{Im}(\eta_r)\approx-1$], so that eventually the Raman field is no longer near a dressed cavity resonance and is not supported. When the Raman ceases, the pump also ceases because in the absence of the Raman field the pump phase shift is not sufficiently bleached to allow the pump to be supported by the cavity at this frequency. Each of the features discussed here can be seen clearly in the experimental plot of Fig. 3.

The mechanisms discussed above provide the basis for understanding the form of the Raman frequency combs. First, there must be sufficient Raman gain, which requires an intracavity pump field amplitude $\alpha\approx1$ or larger for the decay rate parameters we have chosen. Above this value of α, the maximum gain is relatively constant, but the value of $|\Delta|$ at which it occurs depends almost linearly on α. For example, the maximum gain for $\alpha=2$ is 0.26 and occurs near $|\Delta|=90$, while for $\alpha=8$, the maximum gain is 0.30 and occurs near $|\Delta|=330$. Clearly, then, Raman lasing cannot occur in the very far wings of the line, since the largest intracavity pump amplitude possible α_s cannot produce sufficient gain. Near the center of the comb scan (i.e., near the single-photon pump resonance frequency) there is insufficient pump amplitude to produce Raman gain. We note too that even for $\alpha=1$, Raman gain turns to loss for $|\Delta|<39$.

The key element in determining the extent of the Raman comb is the relative phase shift between the pump and the Raman fields. For Raman lasing, these are constrained by Eq. (18), as we can see by noting that at the frequency where the Raman field begins to lase, the pump phase shift $\mathrm{Im}(\eta)\approx\Phi_1$, so that Eq. (18b) becomes

$$\Delta'=\Delta_r-\Delta\approx\mathrm{Im}(\eta_r)-\mathrm{Im}(\eta)+\Phi_{\mathrm{offset}}, \tag{20}$$

where Φ_{offset} $(=\Phi_1-\Phi_2)$ is fixed for a given cavity length. The pump and Raman phase sifts at maximum Raman gain are plotted as a function of pump detuning in Fig. 9, for two different values of pump amplitude. The pump phase shift follows essentially the two-state form (with the proviso that the effective intensity is enhanced by optical pumping to state 2; see Ref. [29]) and so decreases as $1/\Delta$ at large $|\Delta|$ [cf. Eq. (17)]. The Raman phase shift also falls inversely with Δ. So, for fixed value of pump power, the phase-shift difference $[\mathrm{Im}(\eta_r)-\mathrm{Im}(\eta)]$ becomes small at large $|\Delta|$; eventually the term Φ_{offset} dominates in Eq. (20) for Δ'. The width of the gain curve in the (Δ,Δ_r) plane, however, determines how large Δ' may be, as illustrated in Fig. 7(b). For given pump power the Raman gain decreases as $|\Delta|$ becomes large, so that the curves where gain equals loss [Fig. 7(b)] approach each other and Δ' must become small. (For example, with $\alpha=1.5$, Δ' may be in the range of approximately $+1.6$ to -1.6 near $\Delta=-120$, but only in the range of $+0.7$ to -0.7 near $\Delta=-240$.) Thus, in the case of Fig. 6(b), where $\Phi_{\mathrm{offset}}=-5.3$, we see that the Raman field can turn on at low pump power at $\Delta=-100$, while at $\Delta=-240$ the diminished phase-shift difference prevents it from doing so. Even though at large $|\Delta|$ larger pump powers are available than at line center, somewhat offsetting the above effect, Fig. 9(b) shows that there is a corresponding significant further bleaching of the phase-shift difference: Raman lasing at large $|\Delta|$ is forbidden for large Φ_{offset}. Clearly, Raman lasing can begin there with sufficiently high pump power if the magnitude of Φ_{offset} is sufficiently small [as in Figs. 6(c) and 6(d)].

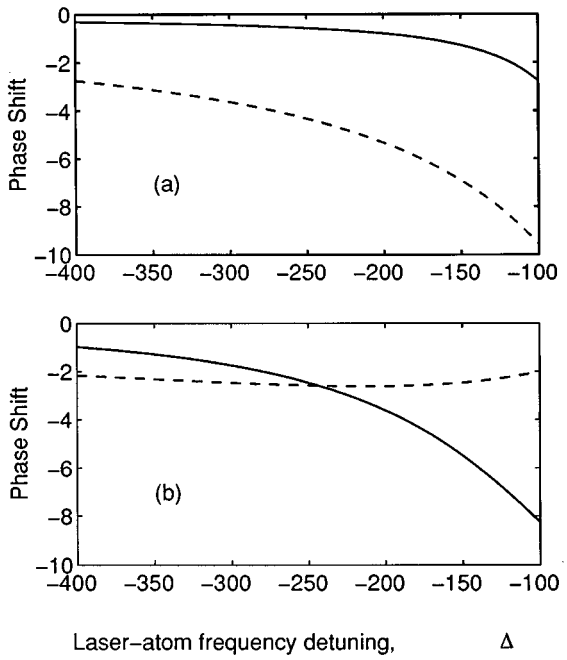

FIG. 9. Phase shifts for the Raman field (solid line) and pump field (dashed line) as a function of pump detuning Δ for the cases (a) $\alpha=1.5$ and (b) $\alpha=8$. In each case, the Raman amplitude is $\beta=10^{-6}$ and at each value of Δ the Raman detuning Δ_r is set to the value that gives the maximum gain. All decay-rate parameters are as for Fig. 6.

We note finally that a large variety of different bistability and switching phenomena have been seen in the numerical modeling [30] and further exploration of these behaviors will be presented elsewhere.

V. CONCLUSIONS

We have observed and characterized properties of the Raman lasing that occurs between the metastable 1*s* levels and the 2*p* manifold of neon, by using a commercial He-Ne laser driven by an external dye laser. Simultaneous bistable optical switching of the pump and up to two different Raman wavelengths has been seen, with a signature strongly dependent on the absolute cavity length. In contrast to most of the previous work on Raman lasing (where the pump amplitude is held constant), in our work modification of the pump intensity plays an important role in the phenomena observed.

A theoretical analysis based on an earlier three-state Raman laser model (e.g., see Ref. [20]), which qualitatively reproduces the experimental results, has enabled us to identify the mechanisms controlling the switching. Some important features of the Raman gain, and the behavior of the pump and Raman phase shifts, have been characterized by examining the Raman-response functions in the presence of the prescribed fields. These properties were then used to explain physically the details of both the single-cavity profile switching and the overall behavior of the Raman frequency combs.

Finally, it is worth mentioning that different wavelengths connecting the 1*s* levels to the 2*p* levels have been used as pump beams and all of the observed Raman lasing lines [22] have shown simultaneously optical-bistable behavior with the pump transmission.

ACKNOWLEDGMENTS

We are indebted to Dr. Alan McCord for assistance in using the AUTO software package and we gratefully acknowledge Dr. Art Phelps and Dr. Derek Stacey for helpful advice and comments on the estimation for various decay rates of neon. W.J.S. wishes to sincerely thank Dr. Peter Hannaford and colleagues for hospitality at the CSIRO Division of Materials Science and Technology, Clayton, Victoria, Australia, where a draft of this paper was prepared. The research is supported by the Research Committee of the University of Otago and the Foundation for Research, Science and Technology under Public Good Science Contract No. UOO 408.

APPENDIX: PARAMETER ESTIMATION

The estimation of the parameters for the model we use is not straightforward. Neon has been the subject of much investigation in atomic and laser physics for many years and although many broadening and transfer rates have been measured, some key parameters for our work have proved difficult to obtain because definitive measurements do not yet appear to have been made. Furthermore, our model ignores a number of important features of the experiment such as inhomogeneous broadening in the gaseous medium and the Gaussian and standing-wave intensity distribution of the laser modes. It is well known (for example, in optical bistability) that even where optical switching behavior is *qualita-*

TABLE I. Parameters for the neon $1s_5 \rightarrow 2p_2 \rightarrow 1s_4$ Raman transition.

Parameters	Estimated	Reference	As used for the modeling
κ_{12}	10–60 MHz	[33]	1.0
κ_1 $(2p_2 \rightarrow 1s_5)$	35.5 MHz	[34,35]	1.1
κ_2 $(2p_2 \rightarrow 1s_4)$	37.6 MHz		0.9
γ_1 $(2p_2 \rightarrow 1s_5)$	1.75 MHz	[36]	0.04
γ_2 $(2p_2 \rightarrow 1s_4)$	0.75 MHz		0.02
Γ_1 $(1s_5 \rightarrow 1s_4)$	0.17 kHz	[37,38]	8.9×10^{-5}
Γ_2 $(1s_4 \rightarrow 1s_5)$	2.08 kHz		10.7×10^{-4}
g_1 $(2p_2 \rightarrow 1s_5)$	1155	[39]	1200
g_2 $(2p_2 \rightarrow 1s_4)$	511		1500
κ	1.5 MHz		0.03

tively unchanged by these simplifications there can be a substantial influence on the ''effective-parameter'' values that allow the model to best reproduce the observed nonlinear behavior [31]. In addition, different physical processes can emerge when the level degeneracy is taken into account: an example is Raman polarization flipping [32]. Our aim in this paper is therefore to show that with reasonable values of the parameters, the model qualitatively reproduces the experimental features we report above.

Perhaps the largest single difficulty is in obtaining a value for the $1s_5 \rightarrow 1s_4$ Raman-coherence decay rate under the conditions of foreign-gas broadening by He. This is hard to measure except in the context of a Raman process. Jabr [33] estimates a value of 15 MHz [half-width at half maximum (HWHM)] for 6 Torr of helium from consideration of the number of consecutive resonant modes. The analysis in Sec. V shows that the nonlinear interaction complicates this argument; however, this estimate gives a reasonable lower limit of 10 MHz (HWHM) at 3 Torr of He. An estimate for the upper limit on κ_{12} can be obtained from the sum of the half-widths of the $1s_4$ and $1s_5$ states, which can be approximated by the widths associated with the $1s_5$-$2p_2$ and $1s_4$-$2p_2$ optical dipoles. Saoudi, Lerminiaux, and Dumont [34] find a foreign-gas (helium) broadening constant of 9.3 MHz/Torr for the $1s_5$-$2p_2$ transition, and we expect that a rate of 10 MHz/Torr is also reasonable for the $1s_4$-$2p_2$ transition. We set forth in Table I our best estimates of the experimental parameters, together with the values (normalized to the Raman-coherence decay rate κ_{12}) used in the modeling.

[1] F. T. Arecchi and A. Politi, Lett. Nuovo Cimento **23**, 65 (1978).
[2] G. P. Agrawal and C. Flytzanis, Phys. Rev. Lett. **44**, 1058 (1980).
[3] G. Grynberg, M. Devaud, and C. Flytzanis, and B. Cagnac, J. Phys. (Paris) **41**, 931 (1980).
[4] J. A. Hermann and B. V. Thompson, Phys. Lett. **79A**, 153 (1980).
[5] G. S. Agarwal, Opt. Commun. **35**, 149 (1980).
[6] M. Reid, K. J. McNeil, and D. F. Walls, Phys. Rev. A **24**, 2029 (1981).
[7] T. Kobayashi, N. C. Kothari, and H. Uchiki, Phys. Rev. A **29**, 2727 (1984).
[8] M. A. Anton, I. Gonzalo, and J. L. Escudero, Opt. Quantum Electron. **21**, 415 (1989).
[9] E. Giacobino, M. Devaud, F. Biraben, and G. Grynberg, Phys. Rev. Lett. **45**, 434 (1980).
[10] N. Peyghambarian, H. M. Gibbs, M. C. Rushford, and D. A. Weinberger, Phys. Rev. Lett. **51**, 1692 (1983).
[11] R. Levy, J. Y. Bigot, B. Honerlager, F. Tomasini, and J. B. Grun, Solid State Commun. **48**, 705 (1983).
[12] A. K. Kar, J. G. H. Matthew, S. D. Smith, B. Davis, and W. Prettl, Appl. Phys. Lett. **42**, 334 (1983).
[13] P. Grangier, J. F. Roch, J. Roger, L. A. Lugiato, E. M. Pessina, G. Scandroglio, and P. Galatola, Phys. Rev. A **46**, 2735 (1992).
[14] M. W. Hamilton, R. J. Ballagh, and W. J. Sandle, Z. Phys. B **49**, 263 (1982).
[15] S. Cecchi, G. Guisfredi, E. Petriella, and P. Salieri, Phys. Rev. Lett. **49**, 1928 (1982).
[16] C. Parigger, P. Hannaford, and W. J. Sandle, Phys. Rev. A **34**, 2058 (1986).
[17] R. G. Harrison and D. J. Biswas, Phys. Rev. Lett. **55**, 63 (1985).
[18] R. G. Harrison, Weiping Lu, and P. K. Gupta, Phys. Rev. Lett. **63**, 1372 (1989).
[19] Weiping Lu and R. G. Harrison, Phys. Rev. A **41**, 6563 (1990).
[20] Weiping Lu and R. G. Harrison, Phys. Rev. A **43**, 6358 (1991).
[21] Zheng Qianbing and Cao Hongli, Chinese Phys. Lett. **4**, 201 (1987).
[22] X.-W. Xia, W. J. Sandle, R. J. Ballagh, and D. M. Warrington, Opt. Commun. **96**, 99 (1993).
[23] W. J. Sandle and A. Gallagher, Phys. Rev. A **24**, 2017 (1981).
[24] J. S. Uppal, R. G. Harrison, and Weiping Lu, J. Mod. Opt. **37**, 605 (1990).
[25] J. C. Ryan and N. M. Lawandy, IEEE J. Quantum Electron. **QE-22**, 2075 (1986).
[26] R. Bonifacio and L. A. Lugiato, Phys. Rev. A **18**, 1129 (1978).
[27] J. C. Englund, R. R. Snapp, and W. C. Schieve, in *Progress in Optics*, edited by E. Wolf (North-Holland, Amsterdam, 1984), Vol. XXI, p. 255.
[28] E. Doedel, AUTO: software for continuation and bifurcation problems in ordinary differential equations. California Institute of Technology, Pasadena, CA (1986).
[29] R. J. Ballagh, J. Cooper, and W. J. Sandle, J. Phys. B **14**, 3881 (1981).
[30] Xiao-wei Xia, Ph.D. dissertation, University of Otago, 1993 (unpublished).
[31] R. J. Ballagh, J. Cooper, M. W. Hamilton, W. J. Sandle, and D. M. Warrington, Opt. Commun. **37**, 143 (1981); see also Ref. [23].
[32] X.-W. Xia, W. J. Sandle, R. J. Ballagh, and D. M. Warrington, in *Quantum Electronics and Laser Science Conference*, Vol. 16 of the 1995 OSA Technical Digest Series (Optical Society of America, Washington, D.C., 1995), p. 169.
[33] S. N. Jabr, Opt. Lett. **12**, 690 (1987).
[34] S. Saoudi, Ch. Lerminiaux, and M. Dumont, Phys. Rev. Lett. **56**, 2164 (1986).
[35] H. G. Kuhn and E. L. Lewis, Proc. R. Soc. London Ser. A **299**, 423 (1967).
[36] P. Hartmetz and H. Schmoranzer, Phys. Lett. **93A**, 405 (1983).
[37] J. D. Clark and A. J. Cunningham, J. Phys. B **16**, 677 (1983).
[38] C. O. Akoshile, J. D. Clark, and A. J. Cunningham, J. Phys. B **18**, 2793 (1985).
[39] g is related through Eq. (8) to the cooperativity and this (for a Fabry-Pérot cavity) is calculated with the same definition as Eq. (2) of Ref. [23]. Note the assumption that *homogeneous* broadening applies. In principle, the theory should take into account the Doppler distribution of resonance frequencies; however, at large detunings and for the relatively high intracavity powers used in the experiment, the approximation of homogeneous broadening is a reasonable one and conveys the essence of the physical behavior (cf. Ref. [23] for the standard optical bistability case).